Clim Dyn (2011) 37:2303–2322
DOI 10.1007/s00382-010-0943-7

Effects of air–sea coupling on the boreal summer intraseasonal oscillations over the tropical Indian Ocean

Ailan Lin · Tim Li · Xiouhua Fu · Jing-Jia Luo · Yukio Masumoto

Received: 27 May 2010 / Accepted: 1 November 2010 / Published online: 21 November 2010
© Springer-Verlag 2010

Abstract The effects of air–sea coupling over the tropical Indian Ocean (TIO) on the eastward- and northward-propagating boreal summer intraseasonal oscillation (BSISO) are investigated by comparing a fully coupled (CTL) and a partially decoupled Indian Ocean (pdIO) experiment using SINTEX-F coupled GCM. Air–sea coupling over the TIO significantly enhances the intensity of both the eastward and northward propagations of the BSISO. The maximum spectrum differences of the northward- (eastward-) propagating BSISO between the CTL and pdIO reach 30% (25%) of their respective climatological values. The enhanced eastward (northward) propagation is related to the zonal (meridional) asymmetry of sea surface temperature anomaly (SSTA). A positive SSTA appears to the east (north) of the BSISO convection, which may positively feed back to the BSISO convection. In addition, air–sea coupling may enhance the northward propagation through the changes of the mean vertical wind shear and low-level specific humidity. The interannual variations of the TIO regulate the air–sea interaction effect. Air–sea coupling enhances (reduces) the eastward-propagating spectrum during the negative Indian Ocean dipole (IOD) mode, positive Indian Ocean basin (IOB) mode and normal years (during positive IOD and negative IOB years). Such phase dependence is attributed to the role of the background mean westerly in affecting the wind-evaporation-SST feedback. A climatological weak westerly in the equatorial Indian Ocean can be readily reversed by anomalous zonal SST gradients during the positive IOD and negative IOB events. Although the SSTA is always positive to the northeast of the BSISO convection for all interannual modes, air–sea coupling reduces the zonal asymmetry of the low-level specific humidity and thus the eastward propagation spectrum during the positive IOD and negative IOB modes, while strengthening them during the other modes. Air–sea coupling enhances the northward propagation under all interannual modes due to the persistent westerly monsoon flow over the northern Indian Ocean.

Keywords Air–sea coupling · Boreal summer intraseasonal oscillations · Tropical Indian Ocean · Interannual variation

A. Lin (✉) · T. Li
Key Open Laboratory for Tropical Monsoon, Institute of Tropical and Marine Meteorology, CMA, Guangzhou, China
e-mail: allin@grmc.gov.cn

T. Li · X. Fu
IPRC, University of Hawaii, Honolulu, Hawaii

T. Li
Department of Meteorology, University of Hawaii, Honolulu, Hawaii

J.-J. Luo · Y. Masumoto
Research Institute for Global Change, JAMSTEC, Yokohama, Japan

1 Introduction

The intraseasonal oscillation (ISO) was first detected by Madden and Julian (1971) using zonal wind over Canton Island. Later they further found that this oscillation is of global scale and is characterized primarily by equatorial eastward propagation with a zonal wavenumber-1 structure and a period of 40–50 days (Madden and Julian 1972; Li and Zhou 2009). Studies have shown that the ISO is one of dominant modes in the tropical atmosphere. The evolution of Asia summer monsoon system (e.g., its break and

active phases) bears a notable ISO characteristic (Lau and Yang 1996; Li et al. 2003a, b). For example, flood damage in East Asia (including heavy precipitation over middle-lower reaches of Yangtze River and South China) links closely to the ISO and its propagation (Shi and Ding 2000; Ju et al. 2005; Lin et al. 2007). The ISO exhibits a multi-scale characteristic (Nakazawa 1988) and may have a two-way interaction with synoptic-scale variabilities (Zhou and Li 2010; Hsu et al. 2010, Hsu and Li 2010). The formation and track of tropical cyclones over the Indian and Pacific Oceans are related to the ISO to some extent (Lin et al. 2004; Zhu et al. 2004).

The ISO exhibits a pronounced seasonal variation (Wang and Rui 1990; Madden and Julian 1994; Li and Wang 1994). While the boreal winter ISO is characterized by eastward propagation along the equator, the boreal summer ISO (BSISO) exhibits a more complex propagation feature, including eastward propagation along the equator, northward propagation over the tropical Indian Ocean and western Pacific, and westward propagation off the equator (e.g., Yasunari 1979; Krishnamurti and Subrahmanyam 1982; Chen and Murakami 1988).

Various studies have been conducted to understand the effects of air–sea coupling on the BSISO (see Wang 2006 for a review). Observational studies (e.g., Webster 1983; Sengupta and Ravichandran 2001; Sengupta et al. 2001; Vecchi and Harrison 2002; Kemball-Cook and Wang 2001) suggested that the intraseasonal SST variability is closely related to the northward propagation of the BSISO. Li et al. (2008) suggested that the SST response to an eastward-traveling ISO may have a delayed impact on the initiation of an ISO event of the opposite phase in the western Indian Ocean. However, it is difficult to identify the cause–effect relations by analyzing observational data alone. Numerical experiments are a more effective way to explore the influence of air–sea coupling on the BSISO. Many previous studies showed that coupled models performed better than their forced atmosphere-only components in terms of the large-scale organization, amplitude and even predictability of the ISO (e.g., Kemball-Cook et al. 2002; Wu et al. 2002; Fu et al. 2003, 2007, 2008; Fu and Wang 2004; Zheng et al. 2004; Seo et al. 2005; Seo et al. 2007). Some other studies, however, suggested that the inclusion of air–sea coupling does not lead to significant improvements in ISO simulations (e.g., Hendon 2000; Inness and Slingo 2003; Bellon et al. 2008; Newman et al. 2009). For example, the study by Seo et al. (2009) showed that the coupled model only slightly outperforms the uncoupled NCEP atmospheric general circulation model (by one to 2 days), suggesting that only limited improvement is gained from the inclusion of the coupled air–sea interaction in the ISO forecast. Thus, further studies are needed to clarify to what degree the results obtained previously are not model-dependent.

As a background state that regulates the ISO activity, the seasonal mean flow and underlying SST exhibit a significant interannual variability over the tropical Indian Ocean (TIO). It has been shown that the interannual variation of SST in TIO exerts marked impacts on the South Asia monsoon (Chang and Li 2000; Ashok et al. 2001; Cherchi et al. 2007) and East Asia monsoon (e.g., Yang and Ding 2007). Using long-term observed monthly SST (1903–1999), Tan et al. (2003) revealed two dominant SST modes in the TIO, one being characterized by a basin-wide pattern (hereafter IOB) and the other a zonal dipole pattern (hereafter IOD). The IOB mode is often driven by Pacific El Niño-Southern Oscillation (ENSO), reaching a maximum basin-wide warming or cooling about 3–4 months after the peaks of El Niño or La Niña (Hong et al. 2010). The IOD is an internal air–sea coupled climate mode in the TIO and usually grows during boreal summer and peaks in fall (Li et al. 2003a, 2003b; Hong et al. 2008a, b). It can be driven by the tropical Pacific ENSO or sometimes occur independently (Luo et al. 2008b, 2010). A positive IOD features anomalous SST cooling in the eastern TIO and weak warming in the west and vice versa for a negative IOD. The TIO basin-wide warming in the summer after an El Niño peak may impact atmospheric circulation anomalies over the western Pacific (e.g., Wu et al. 2009, 2010; Xie et al. 2009). Ajayamohan et al. (2008) and Ajayamohan et al. (2009) suggested that the IOD has a significant impact on the intensity of northward propagating BSISO. The intensity of submonthly variability measured by standard deviation of bandpass-filtered zonal wind fields on the 6–30-day timescale is reduced during positive IOD years (Shinoda and Han 2005). Lin et al. (2010) showed that interannual SST anomalies over the Indian Ocean significantly influence the northward and eastward propagation of the BSISO. The northward propagating BSISO over the central and eastern Indian Ocean weakens (enhances) during the positive (negative) phase of the IOD. The eastward propagating BSISO over the equatorial Indian Ocean and western Pacific enhances (weakens) during the positive (negative) IOB. In this study, we explore to what extent the interannual SST variations over the TIO modify the effect of intraseasonal air–sea coupling on the BSISO by analyzing a pair of 70-year integrations of a coupled atmosphere–ocean model. In the control experiment, the atmosphere and ocean are coupled globally. In the sensitivity experiment, the atmosphere and ocean are not coupled in the TIO, but are coupled elsewhere.

The model and data used in this study are described in Sect. 2. Section 3 assesses the overall impacts of air–sea coupling on the eastward and northward propagations of the BSISO. The physical mechanisms through which air–sea coupling modifies the BSISO are analyzed in Sect. 4.

Section 5 explores how different interannual modes in the TIO modulate the effects of intraseasonal air–sea coupling. Section 6 summarizes our major findings.

2 Model and data

2.1 Model description

The outputs of 70-year simulations with a relatively high-resolution ocean–atmosphere coupled general circulation model (CGCM), named the Scale INTeraction EXperiment-Frontier Research Center for Global Change (SINTEX-F) model (Luo et al. 2003, 2005a), are diagnosed in present study. The SINTEX-F CGCM was developed at the Frontier Research Center for Global Change (FRCGC), based on the original European SINTEX model (Gualdi et al. 2003; Guilyardi et al. 2003). The ocean component is the reference version 8.2 of Océan Parallélisé (OPA; Madec et al. 1998) with the ORCA 2 configuration: an Arakawa-C type grid based on a 2° Mercator mesh. The atmosphere component is the ECHAM4.6 in which a high horizontal resolution (T106) of about 1.1° × 1.1° is used. The coupling fields are exchanged every 2-h between the ocean and atmosphere by means of the Ocean Atmosphere Sea Ice Soil (OASIS) 2.4 coupler (Valcke et al. 2000). Readers are referred to Luo et al. (2005a) for more detailed model descriptions.

This CGCM has been used in various climate studies and predictions. The model realistically reproduced the tropical ENSO, IOB, and IOD modes (e.g., Gualdi et al. 2003; Yamagata et al. 2004; Luo et al. 2005a). Seasonal hindcast experiments for the past 2–3 decades showed skillful prediction of ENSO up to 1–2 years lead (Luo et al. 2005b, 2008a) and IOD up to about 2–3 seasons ahead (Luo et al. 2007). Furthermore, the SINTEX-F CGCM was capable of simulating various propagating modes of the BSISO. For example, the simulated energy spectrum characteristics of meridional propagating BSISO are quite similar to the observed (see Fig. 1). The major observational features of the BSISO, such as its dominant periods, much stronger northward propagation spectrum than southward one over the TIO, SCS and the western Pacific, and minimum spectrum in the Sumatra longitudes (95°–105°E) (e.g., Lau and Chan 1986; Jiang et al. 2004; Lin and Li 2008), are reproduced reasonably well by the CGCM. Figure 2 shows the observed and the model simulated spectrum for zonally propagating BSISO modes. The model is capable of simulating latitude-dependent propagation characteristics—at the equator the eastward propagation is dominated while poleward of 10°N the westward propagation variance is stronger. The overall spectrum distributions for the zonal and meridional propagation modes are quite similar between the simulations and observations despite some discrepancies such as the overestimation of westward propagation north of the equator. Here the observational dataset used in Figs. 1b and 2b is 1979–2003 pentad-mean outgoing longwave radiation (OLR; Liebmann and Smith 1996) obtained from the NOAA-CIRES Climate Diagnostics Center.

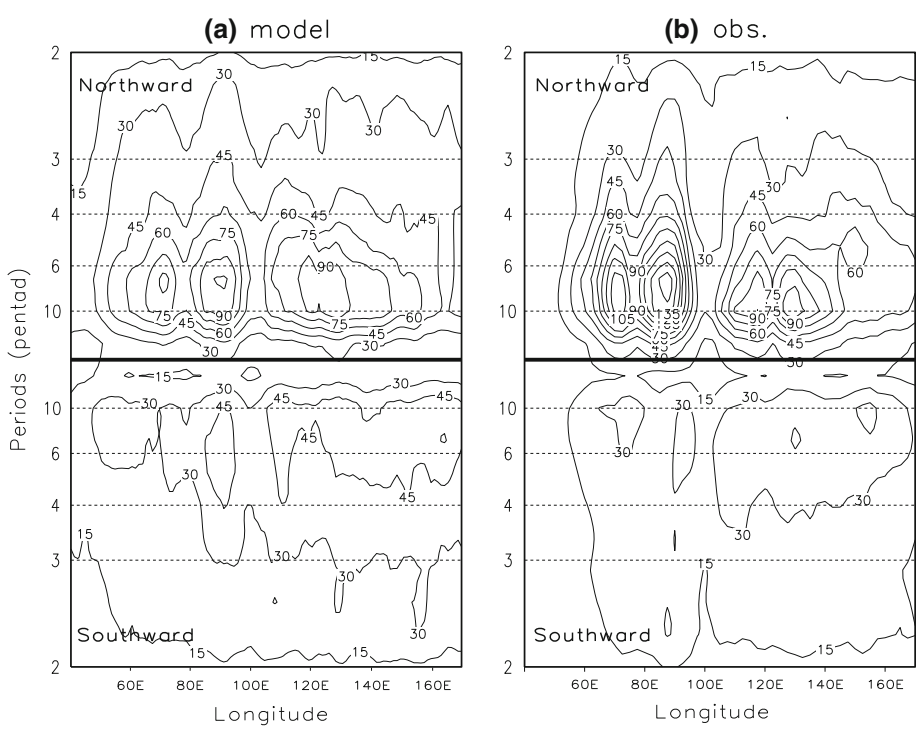

Fig. 1 Spectrum ($W^2\ m^{-4}$) distribution of the northward and southward propagating BSISO as a function of longitude and period for meridional wavenumber-1 (5°S–25°N) from pentad OLR fields of **a** the SINTEX-F CGCM (50-year) and **b** the observation (1979–2003)

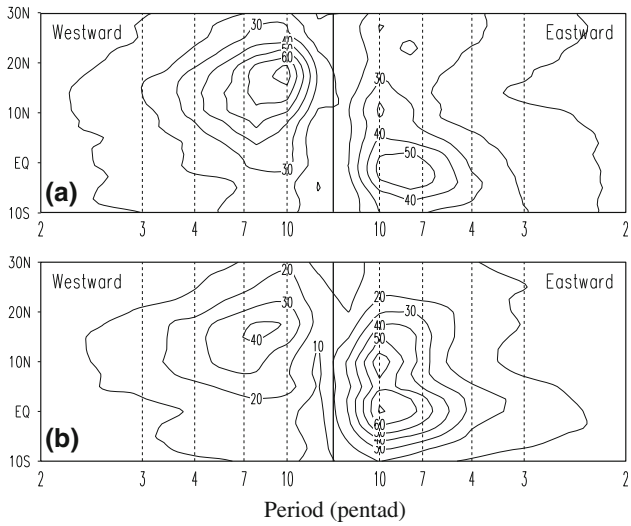

Fig. 2 Spectrum ($W^2\ m^{-4}$) distribution of the westward and eastward propagating BSISO as a function of latitude and period for zonal wavenumber-1 (40°E–180°) from pentad OLR fields of **a** the SINTEX-F CGCM and **b** the observation

In addition to the control run (CTL) described above, in which air–sea coupling is active over all oceans, we carried out a sensitivity experiment in which air–sea coupling in the TIO (30°S–30°N) is suppressed (pdIO). In this case, the atmospheric model is forced by monthly-mean SST over the TIO derived from the CTL run. It is worth noting that the prescribed SST in the TIO in the pdIO experiment is not the climatological SST but has the same interannual variations as in the CTL run. Both experiments are integrated for 70 years started from the same initial conditions. The SST felt by the atmosphere in both experiments is the same in the monthly time scale, but the SST anomaly (SSTA) with timescales shorter than a month is only present in the coupled CTL run. Although the monthly mean SST used in the sensitivity experiment contains a small part of total intraseasonal SST variance, the difference of the ISO variance between monthly-mean and seasonal mean SST is very small (<5%). Therefore, through comparing the two experiments (CTL and pdIO), the effects of intraseasonal air–sea coupling over the TIO on the BSISO can be assessed to a large extent. Excluding the first 20-year spin-up run, we analyze only the last 50-year model outputs.

2.2 Observational data and analysis methods

To assess the reliability of the model simulation, daily averaged OLR data from NOAA-CIRES, at the resolution of 2.5° latitude × 2.5° longitude, is employed as the proxy for convection. To be comparable with the model output, the data is processed into a pentad mean. A finite-domain (5°S–25°N and 40°–90°E) wavenumber-frequency analysis is applied to transform the OLR field from a spatial-time domain to a wavenumber-frequency domain (e.g., Hayashi 1982; Chen et al. 2000; Teng and Wang 2003; Lin and Li 2008). The ISO in present study is defined as variability with oscillating periods of 10–90 days. Because our focus is on the BSISO, all spectrum analysis is conducted for the period from May to October each year. To minimize the effect of discontinuity in the OLR time series, we calculate the spectrum for each summer (May–October) first and then take the mean of individual spectrum over all 50 years. By doing so one does not need to taper the time series at either end. For the limited domain analysis, meridional (zonal) wavenumber-1 corresponds to a wavelength of 30° in latitude (50° in longitude). The annual mean and the first four harmonics are removed from original time series before the wavenumber-frequency analysis is performed. All variables (such as winds, specific humidity, geopotential height, air temperature, SST and OLR) for composite analysis were band-pass filtered to the 10–90-day periods using Morlet wavelet transform (Torrence and Compo1998).

The interannual variations of the TIO SST may be divided into five types: a positive IOD year, a negative IOD year, a positive IOB year, a negative IOB year, and a normal year. The IOD index is defined as the SSTA difference between the western (10°S–10°N, 50°–70°E) and eastern (10°S-EQ, 90°–110°E) Indian Ocean, following Saji et al. (1999). A positive (negative) IOD year is the year when the dipole index exceeds one positive (negative) standard deviation. The IOB index is defined as the sum of the SSTA in the western and eastern Indian Ocean, using the same boxes as for the IOD. The positive (negative) IOB year is selected when the IOB index exceeds 0.7 (−0.7) standard deviation but the IOD index is <1 standard deviation. The normal year is defined as that the IOD (IOB) index is <1 (0.7) standard deviation. The reason for using a lower criterion for the IOB is to increase the sample number for this type of mode in the simulations. Conclusions will not change if one standard deviation is used as criterion for the IOB.

3 Effects of air–sea coupling on the BSISO spectra

The composites of eastward-propagating BSISO spectra calculated based on the zonal wavenumber-1 (corresponding to a wavelength of 50° between 40°E and 90°E) OLR field in the CTL and pdIO and their differences are given in Fig. 3. It is shown that the eastward-propagating BSISO in the CTL is stronger than that in the pdIO. The most significant difference appears around the equator (10°S–10°N) at the periods of 6–10 pentads (Fig. 3c). The northward-propagating BSISO spectrum for the meridional

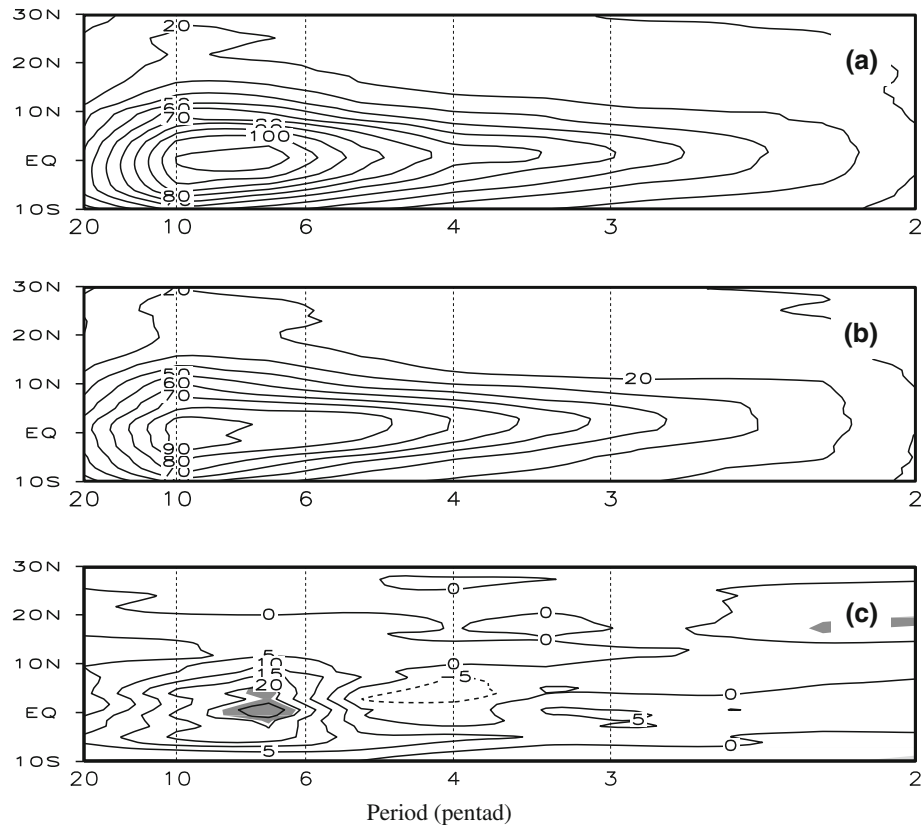

Fig. 3 The composite OLR spectrum ($W^2\ m^{-4}$) of the zonal wavenumber-1 eastward propagating BSISO in **a** the CTL, **b** the pdIO and **c** their differences (CTL − pdIO) during the 50-year period. Shading in (**c**) denotes that the differences exceed the 95% significance level

wavenumber-1 (corresponding to a wavelength of 30°) in the CTL and pdIO and their differences are presented in Fig. 4. The northward-propagating BSISO in the CTL is stronger than that in the pdIO. The largest and significant difference appears in the central and eastern Indian Ocean (65°–95°E) at the periods of 4–10 pentads. The difference of the eastward-propagating (northward-propagating) BSISO spectrum averaged over the latitudinal bands of 10°S–10°N (the longitudinal bands of 65°–95°E) and period bands of 6–10 (4–10) pentads between the CTL and pdIO exceeds 17.0% of the climatological values. The maximum spectrum difference for the eastward- (northward-) propagating BSISO between the CTL and pdIO reaches about 25% (30%) of the climatological values.

The spectrum differences between the air–sea coupled and uncoupled cases over the TIO are quite remarkable even though the monthly SST in the two experiments is the same. This indicates that intraseasonal air–sea coupling over the TIO significantly strengthens the BSISO intensity. The fact that the BSISO intensity is different between the coupled and uncoupled runs over the TIO suggests that stand-alone AGCM run is deficient in the simulations of the BSISO. This finding agrees with previous studies using relatively coarse resolution models or with shorter integration periods (e.g., Flatau et al. 1997; Wang and Xie 1998; Waliser et al. 1999; Zheng et al. 2004; Fu et al. 2003; and Fu and Wang 2004). Checking on a larger longitudinal domain, the air–sea coupling over the TIO enhances the northward-propagating BSISO intensity more efficiently in the Indian Ocean than that in the Pacific (figure not shown).

4 Physical interpretation of the air–sea interaction effect

In this section, we aim to elucidate the physical processes through which intraseasonal air–sea coupling over the TIO affects the eastward and northward propagations of the BSISO, respectively. In the following, a composite analysis approach will be taken by selecting strong eastward (northward) propagation events to reveal their zonal (meridional) structures. Strong eastward (northward) propagation events in the CTL are identified based on the following criterion: The amplitude of the filtered OLR exceeds one standard deviation in a reference longitude (latitude) along 5°S–5°N (70°–95°E). Same number of eastward (northward) propagation events as in the CTL is selected for the pdIO with adjusted criterion. The number of events used to make all composite figures is given in Table 1.

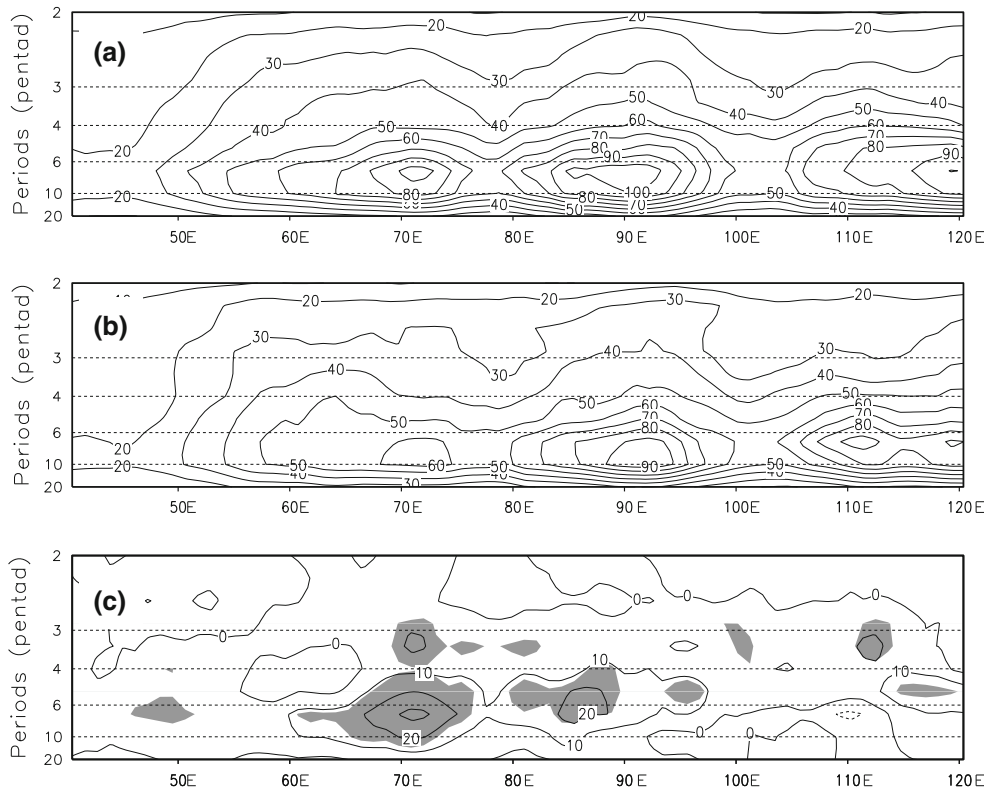

Fig. 4 The composite OLR spectrum ($W^2\ m^{-4}$) of the meridional wavenumber-1 northward propagating BSISO in **a** the CTL, **b** the pdIO and **c** their differences (CTL − pdIO) during the model's last 50-year period. Shading in (**c**) denotes that the differences exceed the 95% significance level

Table 1 The number of events used in each of the composites

Figure number	Convection center	Number of events
Fig. 5	60°, 70°, 80° and 90°E	432
Fig. 6	80°E	97
Fig. 7	60°E	134
Fig. 8	5°N	132
Fig. 9	10 grids between 5°–15°N	1,427
Fig. 10	10 grids between 5°–15°N	1,427
Fig. 11	10 grids between 5°–15°N	1,427
Fig. 15a	60°, 70° and 80°E	347
Fig. 15b	60°, 70°, 80° and 90°E	432
Fig. 15c	60°, 70°, 80° and 90°E	432
Fig. 16	60°, 70° and 80°E	347
Fig. 18	10 grids between 5°–15°N	1,427

4.1 Impact on the eastward-propagating BSISO

The composite of 432 strong eastward-propagating events along the equator in the CTL shows that the ISO convection (represented by OLR) and SST are well coupled and move eastward sequentially: A positive SSTA always locates in the east of the convection center and leads the convection moving eastward (Fig. 5a, b). For a fixed observer at a reference longitude, the SST leads the ISO convection by 1–2 pentads, suggesting a positive feedback from the SST to the convection. Excluding this effect in the pdIO results in a weaker eastward-propagating BSISO convection (Fig. 5c, d). The role of intraseasonal SST in enhancing the eastward-propagating BSISO convection can be seen more clearly in Fig. 5e, f.

Figure 6a shows the composite zonal-vertical cross-sections of the humidity and divergence fields in reference to the convection center at 80°E associated with the eastward-propagating BSISO in the CTL. Note that both the humidity and divergence fields exhibit a clear zonal asymmetry, with the maxima in humidity and 850 hPa convergence located to the east of the convection center. This zonal asymmetry is partially responsible for the eastward propagation of the BSISO over the equatorial Indian Ocean. Figure 6b shows the contrast of zonal distribution of 850-hPa convergence between the CTL (solid line) and the pdIO (dashed line). While there is a clear zonal asymmetry between the 850-hPa maximum convergence and the convection in the CTL, such an asymmetry is weaker in the pdIO. The cause of the wind and divergence differences is argued to be attributed to the effect of the zonal SST asymmetry in the presence of air–sea coupling.

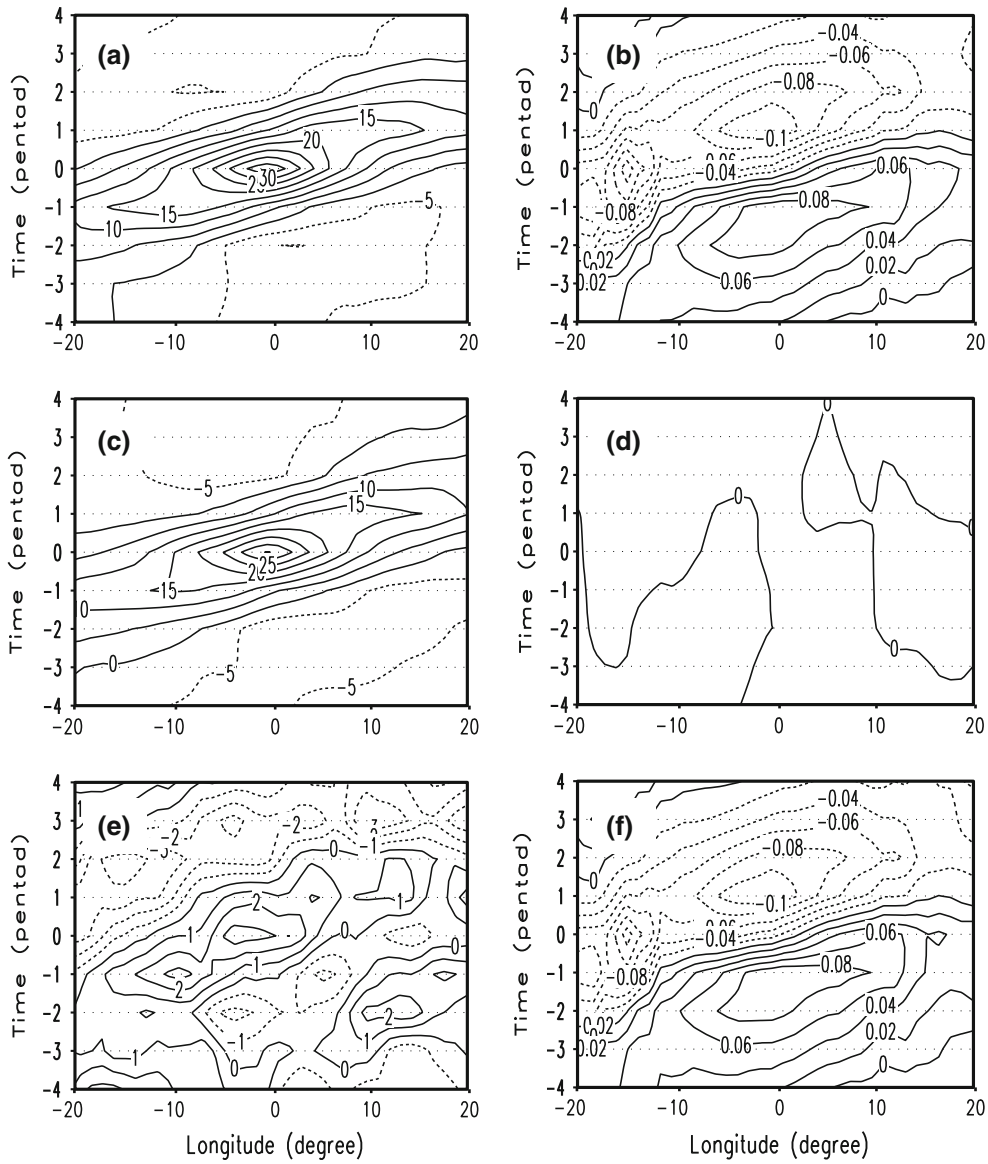

Fig. 5 Composite time-longitude section of the eastward-propagating ISO convection (OLR, unit: W m^{-2}) along the equator in the CTL (**a**) the pdIO (**c**) and their differences (**e**). Composite time-longitude section of the eastward-propagating ISO SST field (unit: K) along the equator with respect to the ISO convection center in the CTL (**b**), the pdIO (**d**) and their differences (**f**). The composite is based on the following longitude locations, 60°, 70°, 80° and 90°E. The abscissa is the relative longitude, with 0 being the ISO convection center

Note that the background low-level zonal wind is westerly over the equatorial Indian Ocean during boreal summer. In response to the ISO convective heating, an easterly (westerly) anomaly appears to the east (west) of the convection center. This leads to the decrease (increase) of total wind speed (solid line in Fig. 6c) and thus reduced (increased) surface evaporation (solid line in Fig. 6d) in the east (west) of the convection center. The asymmetry of surface evaporation, along with enhanced (reduced) downward solar radiation in the east (west) of the convection center, leads to the asymmetric SSTA distribution: A positive (negative) SSTA in the east (west) of the convection center (solid line in Fig. 6e). Anomalous boundary-layer convergence can be generated over the positive SSTA with the mechanism proposed by Lindzen and Nigam (1987), which will lead to further increase of local moisture. The SSTA in Fig. 6e is smaller than that derived from Tropical Rainfall Measuring Mission Microwave Imager (TMI) observations (Joseph and Sabin 2008). The smaller SSTA here is possibly due to a large number of events selected for the composite and/or model deficiencies in describing the observed air–sea interactions.

Excluding air–sea coupling in the Indian Ocean (the pdIO) also produces similar asymmetries on the divergence, humidity, wind speed, and surface evaporation fields (dashed lines in Fig. 6) as in the CTL but with

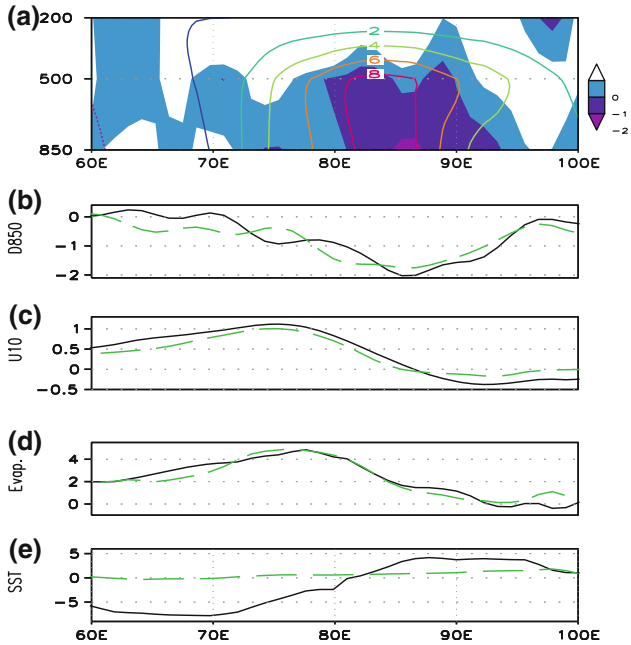

Fig. 6 Structures of the eastward propagating BSISO along the equator in reference to the convection center at 80°E: **a** zonal–vertical profiles of the divergence (10^{-6} s^{-1}) (*shading*) and specific humidity (*contour*) (10^{-4} kg kg^{-1}) in the CTL; the vertical axis is the pressure (hPa); **b–e** 850 hPa divergence (10^{-6} s^{-1}), surface zonal wind at 10-m high, surface evaporation (10^{-9} m s^{-1}), and SST (10^{-2} K) in the CTL (*solid lines*) and the pdIO (*dashed lines*)

weaker amplitudes. The weaker asymmetric amplitudes lead to a weaker eastward-propagating BSISO spectrum in the pdIO than that in the CTL. These results demonstrate the role of air–sea coupling in strengthening the amplitudes of zonal asymmetries in the zonal wind, divergence and moisture fields, so does the eastward propagating BSISO.

The evolutions of the composite OLR from pentad −3 to pentad +3 are given in the Fig. 7, which is composed from 134 strong eastward-propagating BSISO events in both CTL and pdIO. The reference time (pentad 0) corresponds to the time when the BSISO convection center reaches 60°E. In the CTL run (left panel of Fig. 7), the BSISO convection appears in the equatorial western Indian Ocean (about 50°E) at pentad −3. In the following pentads, the convection gradually intensifies and moves eastward along the equator. At pentad 0, the convection arrives at 60°E and reaches a maximum intensity. At pentad 1, a negative convection center appears over the western equatorial Indian Ocean and eastern Africa. The ISO convection then weakens as it moves eastward. At pentad +3, the convection center arrives in the eastern Indian Ocean. A remarkable feature in the left panel of Fig. 7 is that warm SST anomalies are always located to the east or northeast of the convection.

The most evident difference between pdIO (right panel of Fig. 7) and CTL is the timing of occurrence of a positive convective perturbation in the equatorial western Indian Ocean. The positive convective perturbation doesn't appear until pentad −1, whereas it appears at pentad −3 in CTL. The convection in pdIO is weaker than that in CTL at pentad 0 and it is hardly discerned at pentad +3. The differences between the left and right panels of Fig. 7 demonstrate the impact of air–sea coupling over the TIO in strengthening the eastward-propagating BSISO.

4.2 Impact on the northward-propagating BSISO

In this section we aim to unveil the physical processes through which air–sea coupling enhances the northward-propagating BSISO spectrum.

4.2.1 Structure changes of the northward-propagating BSISO

The composite of 132 strong northward-propagating BSISO events is constructed from the CTL run. The reference time (pentad 0) corresponds to the time when the BSISO convection center reaches 5°N along the longitudinal band 70°–95°E. The spatial–temporal evolutions of the composite OLR from pentad −3 to pentad +3 are given in the left panel of Fig. 8. At pentad −3, the BSISO convection appears in the equatorial western Indian Ocean (about 50°E). In the following pentads, the convection gradually intensifies and moves eastward along the equator. At pentad −1, the convection moves to the eastern equatorial Indian Ocean. After that, the convection starts to shift northward while intensifying. At pentad 0, the convection arrives at 5°N and reaches a maximum intensity. Meanwhile, a negative convection center appears over the western equatorial Indian Ocean. The ISO convection then weakens on the course northward. At pentad +2, the convection center arrives at the northern Bay of Bengal and its vicinity.

A remarkable feature in the left panel of Fig. 8 is that warm SST anomalies are always located to the northeast or north of the convection. This feature is consistent with the observations (e.g., Wang et al. 2006; Seo et al. 2007) and related to air–sea coupling, which will be discussed later.

The right panel of Fig. 8 illustrates a similar spatial–temporal evolution of the composite BSISO from the pdIO run. The most evident difference between the pdIO and CTL is the timing of occurrence of a positive convective perturbation in the equatorial western Indian Ocean. The positive convective perturbation doesn't appear until pentad −2, whereas it appears at pentad −3 in the CTL. The convection in the pdIO is slightly weaker than that in the CTL at pentad 0. It is also found that the convection decays much faster on its course northward so that it totally disappears at pentad +3. The differences between the left and right panels of Fig. 8 demonstrate that air–sea coupling

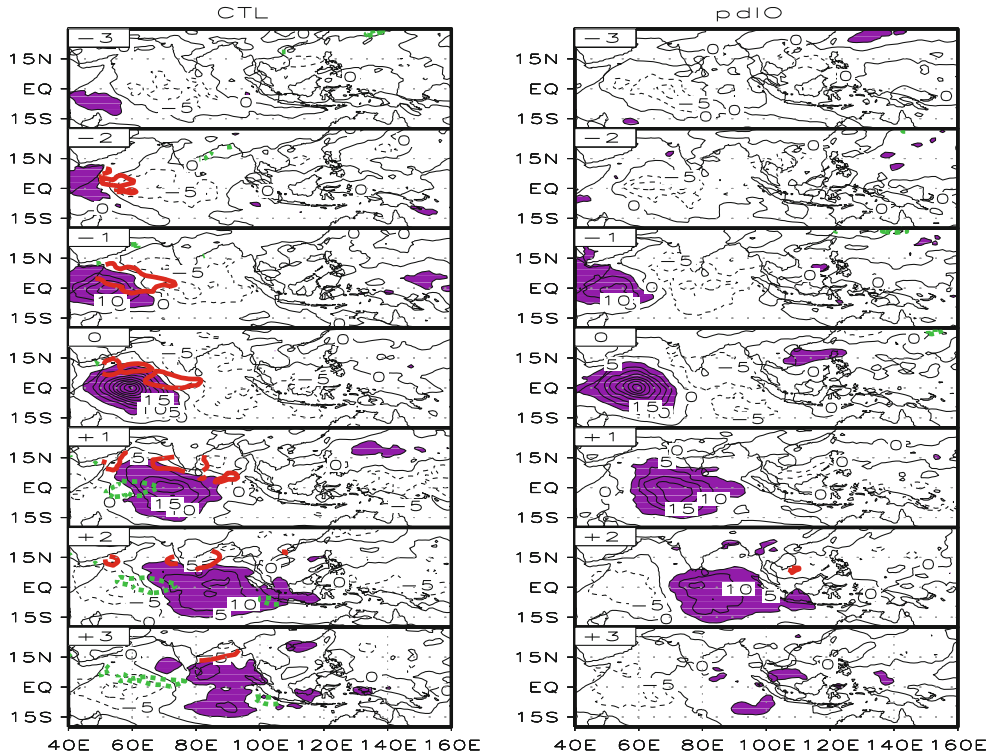

Fig. 7 (Left panel) Composite evolution of the eastward propagating BSISO convection (OLR, thin contour, W m^{-2}) and SST (*thick contour*, K) anomalies from pentad −3 to pentad +3 in the CTL. Pentad 0 is a reference time when the convection center moves to 60°E along equator. *Shading* represents convection (OLR) anomalies greater than or equal to 5 W m^{-2}. The SST contours of 0.08 K (−0.08 K) are highlighted by *red thick solid* (*green dashed*) *lines*. *Right panel* same as the *left panel* except for the convection (OLR) anomalies in the pdIO

over the TIO strengthens the northward-propagating BSISO.

To further illustrate the differences of the northward-propagating BSISO between the CTL and the pdIO, we compare the meridional-vertical structures of the BSISO from these two runs (Fig. 9). The vertical structures are composed with 1,427 strong BSISO events at various latitudes within 5°–15°N. Both the CTL and pdIO capture the meridional asymmetries of the relative vorticity and humidity fields relative to the BSISO convection center. The maximum low-level vorticity and humidity are located north of the convection center, consistent with the observations (Jiang et al. 2004). The associated perturbations in the pdIO are weaker than that in the CTL.

The time-latitude evolution of SSTA with respect to the BSISO convection shows that there are clear temporal and spatial lagged relationships between the convection and SSTA in the CTL (Fig. 10a, b). The maximum (minimum) SSTA locates to the north of and is earlier than a positive (negative) convection center. At a given latitude, the maximum SSTA appears 2 pentads earlier than the maximum convection. This result is consistent with the previous observational analyses (e.g., Webster 1983; Sengupta et al. 2001). Same as the eastward-propagating case (Fig. 5), air–sea coupling significantly increases the strength of the northward propagating BSISO (Fig. 10e, f).

Figure 11a presents the composite meridional–vertical structures of humidity and convergence associated with the northward-propagating BSISO in the CTL. The meridional asymmetry of both the humidity and convergence fields is similar to the zonal asymmetry in the eastward-propagating case (Fig. 6). The maxima of the humidity and convergence locate in the north of the BSISO convection. Figure 11b shows the distribution of 850-hPa convergence in both the CTL and pdIO. Compared to that in the pdIO, the maximum 850-hPa convergence in the CTL is slightly enhanced and shifts further northward. The asymmetry of the divergence in pdIO is partially caused by the asymmetry of cyclonic vorticity at top of the planetary boundary layer through Ekman pumping process. The air–sea coupling, on the other hand, may also contribute to this divergence asymmetry, through induced SSTA gradients (Lindzen and Nigam 1987).

As the boreal summer low-level zonal wind over the northern Indian Ocean is westerly, an easterly (westerly) anomaly to the north (south) of the convection results in a weakened (enhanced) wind speed and thus a decreased (increased) surface evaporation (Fig. 11d). Therefore, a positive (negative) SSTA is generated to the north (south)

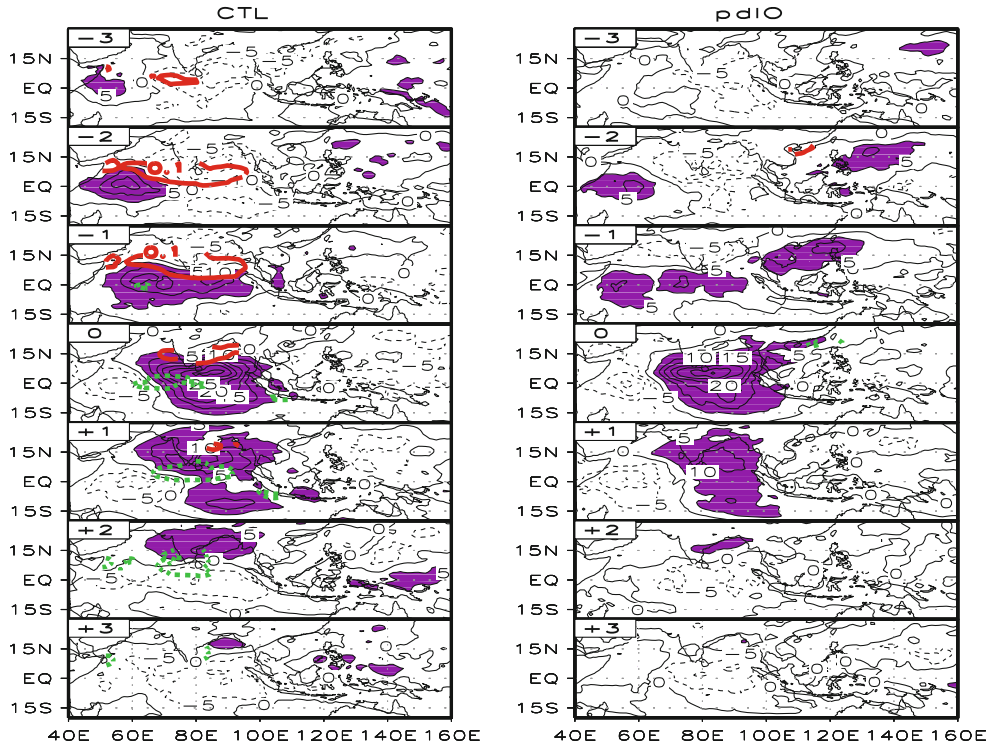

Fig. 8 *Left panel*: composite evolution of the northward propagating BSISO convection (OLR, *thin contour*, W m^{-2}) and SST (*thick contour*, K) anomalies from pentad −3 to pentad +3 in the CTL. Pentad 0 is a reference time when the convection center moves to 5°N along 70°–95°E. *Shading* represents convection (OLR) anomalies greater than or equal to 5 W m^{-2}. The SST contours of 0.1 K (−0.1 K) are highlighted by *red thick solid* (*green dashed*) *lines*. *Right panel* same as the *left panel* except for the convection (OLR) anomalies in the pdIO

of the convection (Fig. 11e). The warm SSTA-induced low surface pressure would, in turn, favor the boundary-layer convergence (Lindzen and Nigam 1987) and thus the increase of the boundary layer humidity, enhancing the northward propagation of the BSISO. The suppression of interactive air–sea coupling weakens the northward-propagating BSISO in the pdIO.

4.2.2 *Effects of background mean state changes*

As found in Jiang et al. (2004), the vertical shear of zonal mean flow and the meridional distribution of background moist static energy are crucial atmospheric factors that cause the northward propagation of the BSISO. The differences of the zonal wind vertical shear (u_{850}–u_{200}) between the CTL and pdIO (Fig. 12a)shows an increase of the monsoon easterly shear in the CTL over the northeastern Indian Ocean where the northward propagation is pronounced (see Fig. 1). The increased easterly shear may enhance the asymmetric vorticity perturbation north of the convection, helping the northward shift of the boundary-layer moisture convergence and resulting in stronger northward propagation of the convection (Jiang et al. 2004; Drbohlav and Wang 2005; Wang et al. 2006). This basic state change contributes to enhance the northward-propagating BSISO over the Bay of Bengal.

Figure 12b shows that the background specific humidity increases significantly over the Bay of Bengal in the CTL. This humidity increase helps strengthen the meridional moisture gradient between the equator and the northern Indian Ocean. With this enhanced meridional humidity gradient, the southward flow in response to the BSISO convection can transport more moisture to the northern side of the convection (Jiang et al. 2004), which enhances the meridional asymmetry of the humidity and thus strengthens the northward-propagating BSISO. Again, this effect primarily works in the eastern Indian Ocean rather than the western Indian Ocean, where the change of the background moisture gradient is insignificant (Fig. 12b). Some other components of the mean flow have also been identified to be important for the northward propagation, such as the vertical shear of the meridional wind and the intensity of the monsoon jet (Bellon and Sobel 2008). Compared to the pdIO, the monsoon westerly jet is stronger in the CTL (see Fig. 12c). The change of vertical shear of the meridional wind, however, is not significant.

The above analyses reveal three possible ways through which air–sea coupling in the TIO can enhance the

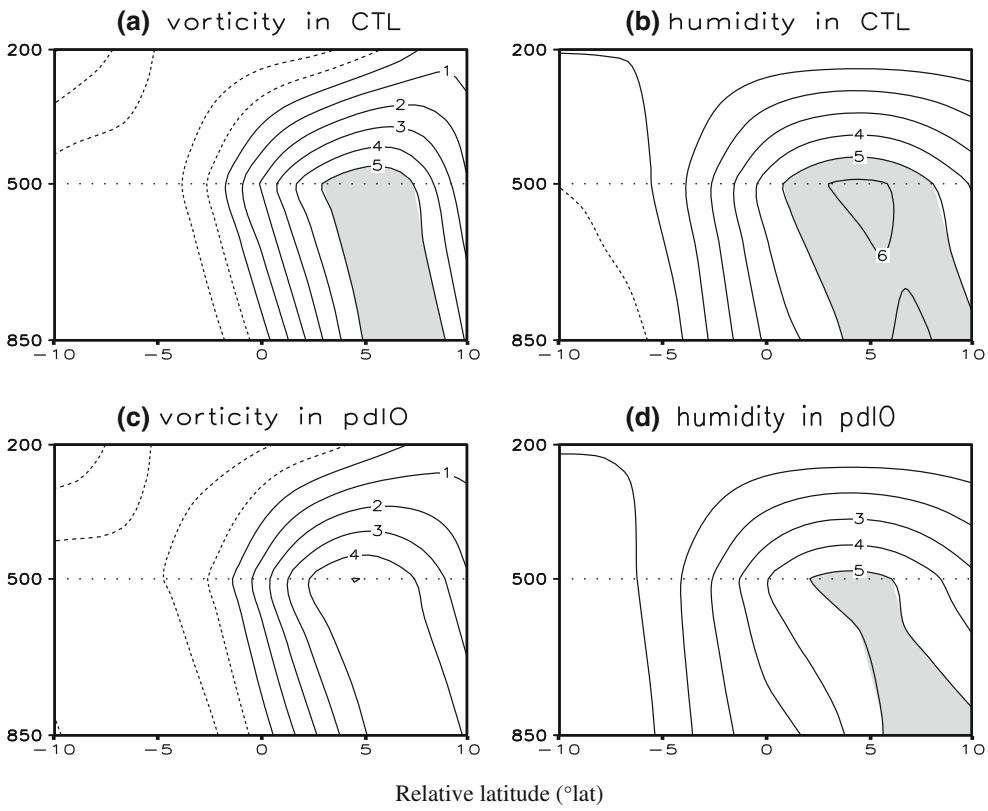

Fig. 9 Composite meridional–vertical structures of the northward propagating BSISO along 65°–95°E: **a** vorticity (10^{-6} s^{-1}) in the CTL, shading is greater than or equal to 5; **b** specific humidity (10^{-4} kg kg^{-1}) in the CTL, *shading* is greater than or equal to 5; **c–d** as in (**a–b**), but the results from the pdIO run. *Horizontal axis* is the relative latitude (°lat) with respect to the ISO convection center. The *vertical axis* is the pressure (hPa)

northward propagation of the BSISO. First, the air–sea interaction generates a positive SSTA north of the BSISO convection, which leads to an enhanced boundary layer convergence and thus an increase in the boundary layer moisture. The latter further enhance convective instability and lead the convection to move northward. Second, air–sea coupling increases the mean vertical shear of zonal wind, mean meridional moisture gradient and monsoon westerly over the Bay of Bengal (Fig. 12), all of them favor the northward-propagating BSISO. Third, because the northward propagation closely connects to the eastward-propagating BSISO (Wang and Xie 1997; Jiang et al. 2004), the amplitude and frequency increases of the eastward-propagating BSISO due to air–sea coupling further enhance the northward propagation.

5 Dependence of air–sea coupling effects on Indian Ocean dipole and basin modes

The overall effects of intraseasonal air–sea coupling on the BSISO over the 50-year period have been studied in the previous sections. In this section, we investigate how the air–sea coupling effects will be changed by the interannual variations of the TIO SST.

5.1 Modulation on the eastward-propagating BSISO

An index is introduced to measure the intensity of the eastward-propagation mode over the equatorial Indian Ocean (hereafter IEPMIO). The IEPMIO is defined as the wavenumber-1 OLR spectrum averaged over 10°S–10°N and a period band of 6–10 pentads. The selection of the averaged domain is based on the climatological spectrum distribution (Fig. 3a) and the region of statistically significant spectrum differences between the CTL and pdIO (Fig. 3c). The IEPMIO differences between the CTL and pdIO exhibit large interannual variations. The standard deviation of 50-year time series of the IEPMIO differences reaches about 47 (W m^{-2})^2. It is much larger than the mean difference value between the CTL and pdIO, which is about 15 (W m^{-2})^2. It is noted that the IEPMIO differences are negative in some years. This indicates that intraseasonal air–sea interaction does not always enhance the intensity of the eastward-propagating BSISO over the equatorial Indian Ocean although the climatological mean effect does.

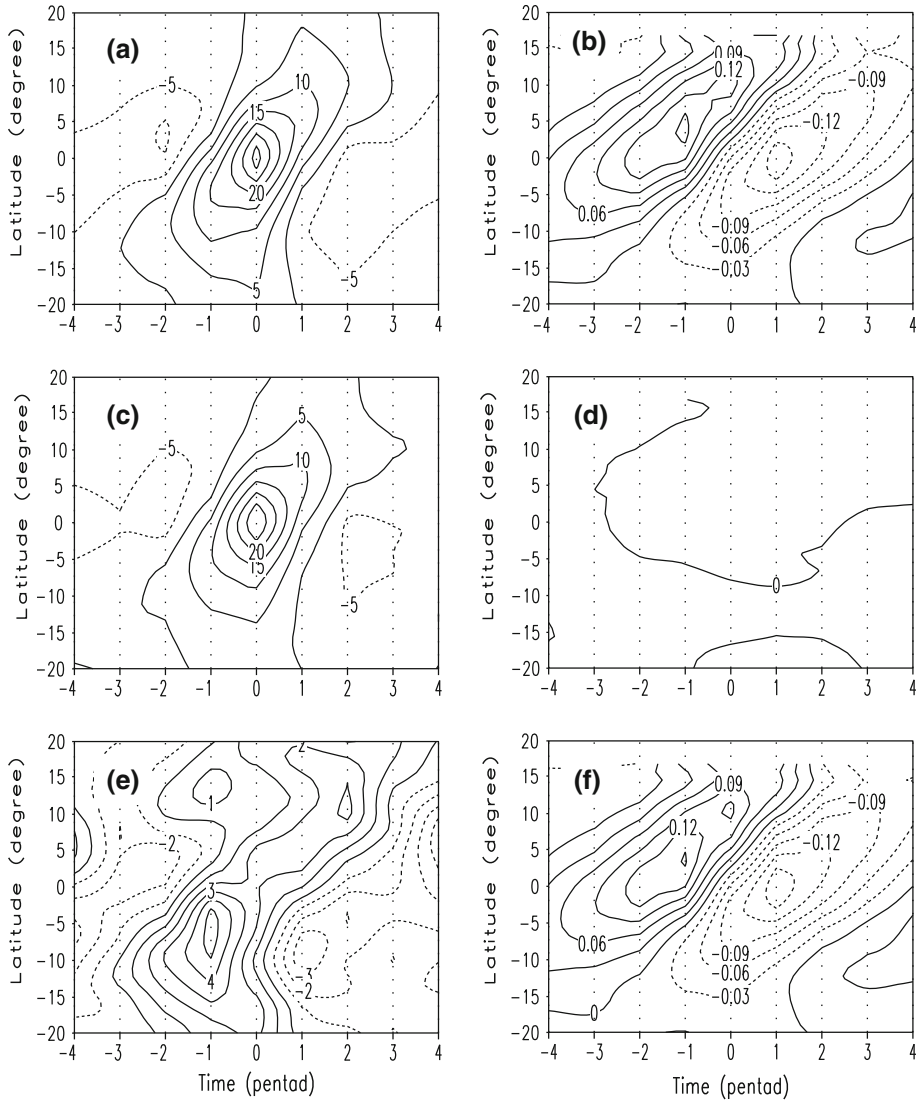

Fig. 10 Composite time-latitude section of the northward-propagating ISO convection (OLR, unit: W m^{-2}) along 65°–95°E in the CTL (**a**), the pdIO (**c**) and their differences (**e**); Composite time-latitude section of the northward-propagating ISO SST field (unit: K) along 65°–95°E with respect to the ISO convection center in the CTL (**b**), the pdIO (**d**) and their differences (**f**). The composite is based on multi latitudinal locations of the convection center within 5°–15°N. The abscissa is the relative time, with 0 being the strongest ISO convection

To examine how the effect of intraseasonal air–sea coupling depends on the interannual modes of the TIO SST anomalies, we divide TIO interannual SST variations into five groups: a positive IOD condition, a negative IOD condition, a positive IOB condition, a negative IOB condition and a normal condition (each condition is defined in Sect. 2). The IEPMIO differences between the CTL and pdIO (the dashed line in Fig. 13) are composed based on these five groups. Note that the differences are positive during the negative IOD year, positive IOB year and normal year, but negative during the positive IOD year and negative IOB year. The differences for the entire 50 years, the positive IOB years and the normal years exceed the 95%, 90% and 95% confidence level, respectively. This points out that the interannual SST variability in the TIO significantly modulates the effect of intraseasonal air–sea coupling on the eastward-propagating BSISO.

How does the interannual SST variability modulate the intraseasonal air–sea coupling process? Figure 14 shows that the boreal summer mean zonal winds on the equator (solid lines) are westerly in the negative IOD year, positive IOB year and normal year, but weak easterly in the positive IOD and negative IOB years. As discussed in previous sections, the effect of air–sea coupling on the eastward-propagating BSISO depends on the background zonal winds. Under a normal westerly condition, a Kelvin-wave response to the east of the BSISO convection acts to reduce the surface wind speed and warm the sea surface; the resultant positive SSTA to the east of the convection favors the boundary-layer convergence and humidity increase, leading to the eastward propagation of the BSISO convection. However, the above coupling effect would be reversed when the background westerly changes to easterly. The change of the background zonal wind is closely related to the zonal gradient of the SST (Fig. 14, gray bar).

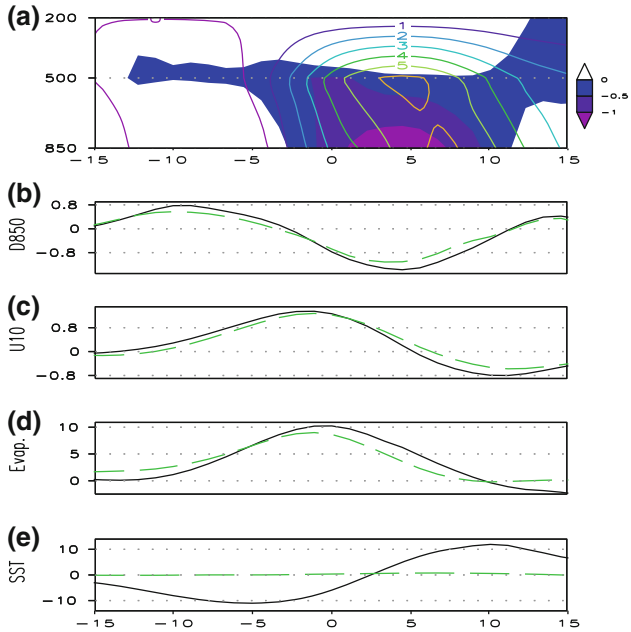

Fig. 11 Structures of the northward propagating BSISO along 65°–95°E with respect to the ISO convection center: **a** meridional–vertical structures of specific humidity (*contour*) (10^{-4} kg kg^{-1}) and divergence (*shading*) derived from the CTL; the vertical axis is the pressure (hPa); **b** divergence (10^{-6} s^{-1}) at 850 hPa in the CTL (*solid line*); **c** zonal wind at 10-m (m s^{-1}) in the CTL (*solid line*); **d** surface evaporation (10^{-9} m s^{-1}) in the CTL (*solid line*); and **e** sea surface temperature (10^{-2} K) in the CTL (*solid line*). **b–e** *dashed line* as *solid line*, but the results from the pdIO run. The composite is based on multi latitudinal locations of the convection center within 5°–15°N

The positive SST gradient during the negative IOD years enhances the equatorial westerly (Li et al. 2003a, 2003b). In contrast, the negative SST gradient during the positive IOD causes an easterly background wind. During a positive (negative) IOB year, the background westerly is strengthened (weakened), possibly due to enhanced (suppressed) Indian monsoon heating (Chang and Li 2000, Li et al. 2001, Li and Zhang 2002). Physically, it is argued that a basin-wide warming during a positive IOB may lead to the increase of surface evaporation and thus the increase of surface moisture prior to the monsoon onset. Once the monsoon onsets, the mean monsoon circulation may bring the anomalous moisture into the monsoon region and leads to enhanced monsoon heating and low-level westerly.

The change of the background zonal wind associated with the interannual SST variability in the TIO may modulate the amplitude of the intraseasonal SSTA. Figure 15a shows that the amplitude of the intraseasonal SSTA is greater during the negative IOD and positive IOB events. It is also interesting to note that averaged over 5°S and 5°N, the SSTA always peaks at the east side of the ISO convection, no matter what interannual modes appear. To understand this feature, we plot the horizontal maps of the composite SSTA (composite was made for the ISO convection being located in the central equatorial Indian Ocean) for each mode (see Fig. 16). Although the zonal wind at the equator changes from westerly to easterly or near zero in the positive IOD and negative IOB summers, the surface westerly is pronounced north of the equator for all the modes (see Fig. 17). The easterly anomalies to the east of the ISO convection result in a decrease of the surface wind speed and thus a decrease of surface evaporation north of the equator, which causes a warm SSTA. South of the equator, the easterly anomalies reinforce the background easterly, resulting in a cold SSTA. However, this cooling effect is much smaller because the ocean mixed layer depth is much deeper south of the equator than north of the equator (Fu et al. 2003). Besides, the cooling effect is offset by warm ocean advection by anomalous mixed-layer currents. This is why the maximum warming appears north of the equator. This explains why the averaged SSTA between 5°S and 5°N is always positive to the east of the ISO convection for all interannual modes in the TIO.

Figure 15b and c further illustrate the zonal distributions of 850-hPa specific humidity field during the five modes in CTL and pdIO. Note that in both the CTL and pdIO experiments the specific humidity perturbation exhibits a zonal asymmetry characteristic, with a greater positive humidity anomaly located to the east of the convection center. It is also interesting to note that compared to CTL, the humidity asymmetry in pdIO increases during the positive IOD and negative IOB modes. Under the other modes, the zonal asymmetry decreases. This explains why air–sea coupling causes the decrease of the eastward propagation spectrum during the positive IOD and negative IOB events. The decrease of the low-level humidity to the east of the convection center due to air–sea coupling during the two modes is attributed to the wind-evaporation-SST feedback in the presence of the mean easterly at the equator. In pdIO, a local anomalous easterly increases the surface evaporation and thus the near surface humidity. In CTL with air–sea coupling involved, the enhanced surface evaporation leads to a local cooling, which further reduces the surface evaporation through the modulation of the sea–air specific humidity difference. As a result, air–sea coupling tends to decrease of the low-level humidity. The opposite coupling effect happens when the equatorial westerly is pronounced during the other modes. Therefore, the simulation results demonstrate that the impact of the air–sea coupling on the eastward-propagating BSISO is greatly modulated by the interannual variation of the TIO.

5.2 Modulation on the northward propagating BSISO

Similar to the zonal-propagating mode, another index is introduced to measure the intensity of the northward-propagating BSISO over the TIO (INPMIO). The INPMIO

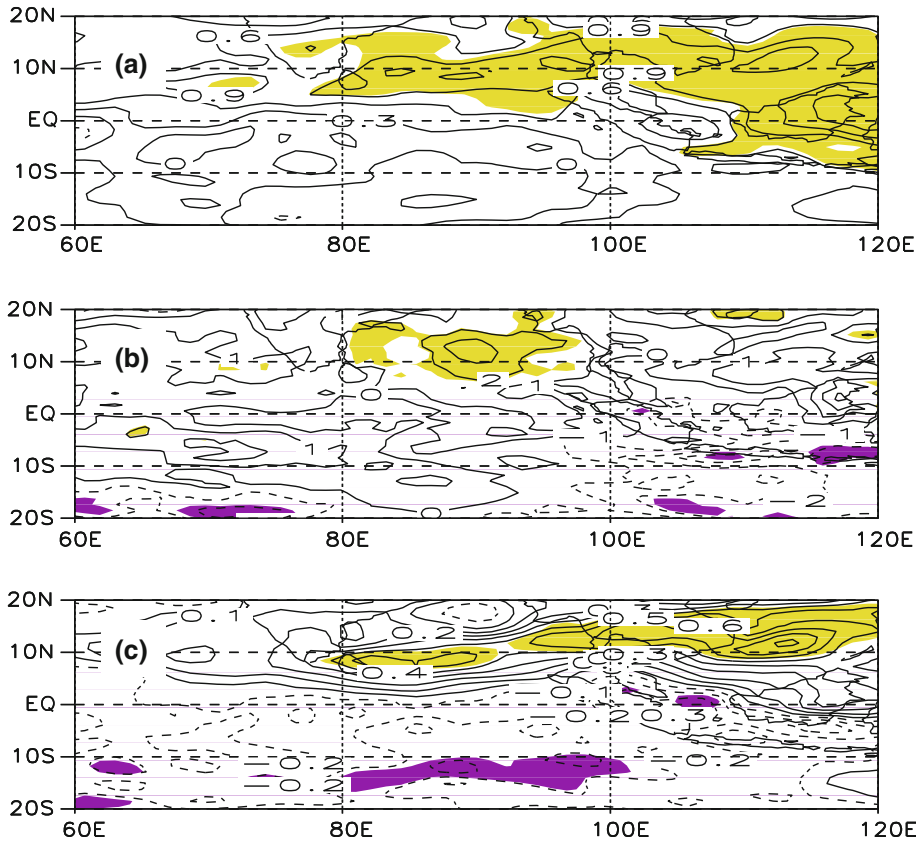

Fig. 12 Differences between the CTL and the pdIO of **a** vertical shear of zonal wind (u_{850}–u_{200}) (m s^{-1}), **b** 850-hPa specific humidity (g kg^{-1}) and **c** 850-hPa zonal wind (m s^{-1}) during the 50-year period. *Shading* denotes that the difference exceeds the 95% significance level

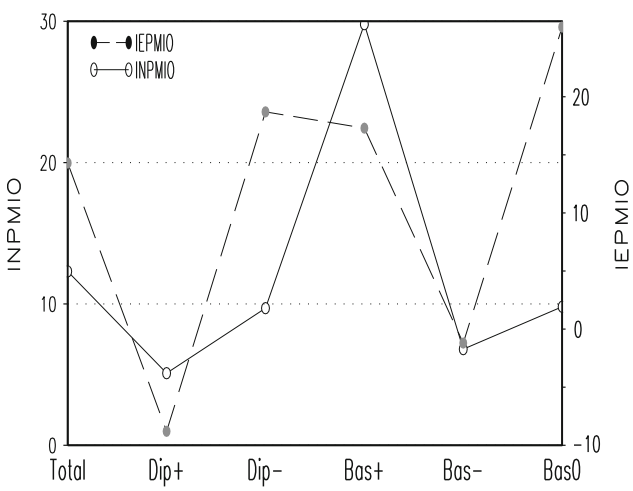

Fig. 13 The IEPMIO (*dashed line*) and INPMIO (*solid line*) power spectrum differences between the CTL and the pdIO for different interannual SSTA modes over the TIO. Sign deputy along horizontal axis: Total, ~50 year; Dip+, ~positive IOD mode; Dip−, negative IOD mode; Bas+, ~positive IOB mode; Bas−, ~negative IOB mode; Bas0, ~normal year

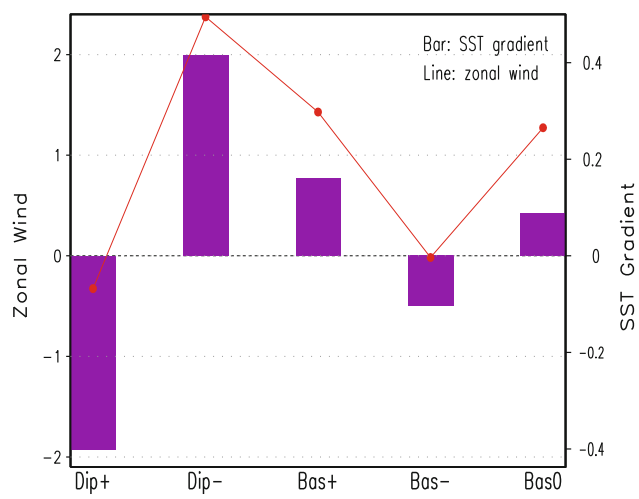

Fig. 14 The background 10-m zonal wind (m s^{-1}) averaged over 65°–95°E and zonal SST gradient along the equatorial (5°S–5°N) Indian Ocean (difference between 85°–95°E and 65°–75°E, unit: K) composed based on different interannual SSTA modes

is defined as the wavenumber-1 OLR spectrum averaged over the longitudinal band of 65°–95°E for the period of 4–10 pentads. The INPMIO differences between the CTL and pdIO also exhibit large interannual variations. The standard deviation of 50-year time series of the INPMIO differences is 23 (W m^{-2})^2, which is much larger than the mean INPMIO differences between the CTL and pdIO [12.3 (W m^{-2})^2].

The effect of the TIO interannual variation in regulating the air–sea coupling effect on the northward-propagating BSISO is quantitatively described in Fig. 13 (solid line).

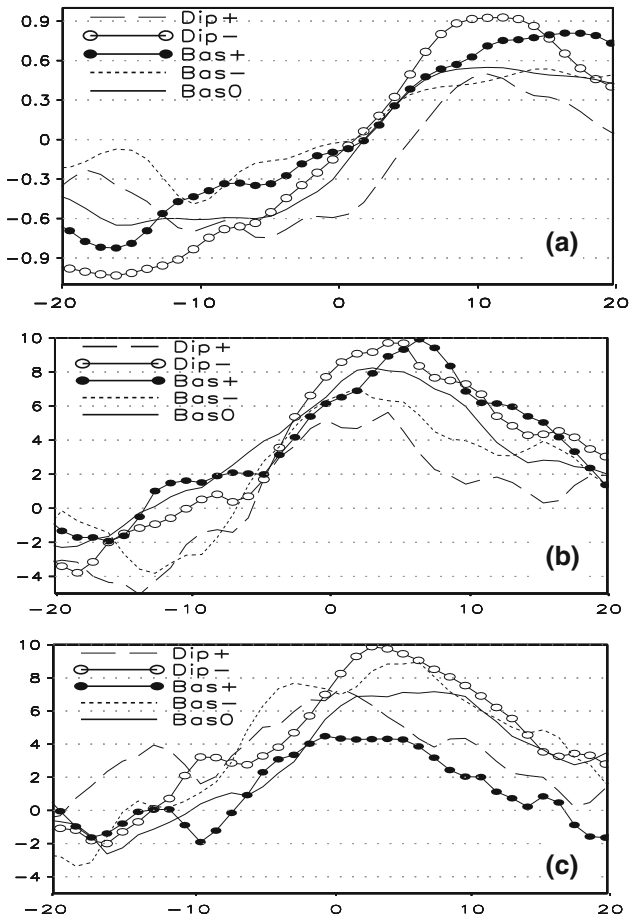

Fig. 15 **a** Composite zonal distribution of SSTA (10^{-1} K) along the equator (5°S–5°N) with respect to the ISO convection center at 60°, 70° and 80°E for different interannual modes of the TIO. **b** Composite zonal distribution of 850-hPa specific humidity (10^{-4} kg kg^{-1}) anomaly along the equator (5°S–5°N) with respect to the ISO convection center at 60°, 70°, 80° and 90°E for different interannual modes of the Indian Ocean SSTA in the CTL. **c** Same as (**b**) but for pdIO. Abscissa in **a**, **b** and **c** is the relative longitude (°) with respect to the convection center

Different from the eastward-propagating case, air–sea coupling acts to enhance the northward-propagating BSISO under all the interannual modes. This is because the key background variable that affects the air–sea coupling effect over the northern Indian Ocean is the low-level westerly, which does not change sign under the five modes (Fig. 17). As a result, the air–sea coupling always strengthens the northward-propagating ISO in boreal summer. The other background fields (e.g., vertical easterly shear, the meridional gradient of moisture) also maintain the favorable distributions for the northward propagation of the BSISO.

The extent to which the northward propagating BSISO spectrum is modulated, however, depends on the phase of the IOD. The northward propagating BSISO over the central and eastern Indian Ocean weakens (enhances) during the positive (negative) phase of the IOD, consistent with Ajayamohan et al. (2008, 2009). It is noted from Fig. 13 (solid line) that the INPMIO difference between the CTL and pdIO is greatest during the positive IOB years. The difference exceeds the 99% confidence level during the positive IOB years and during the entire 50 years, whereas it only exceeds the 90% confidence level during the normal years.

Figure 18 shows the evolutions of the composite ISO convection (solid line) and SST (dashed line) under different interannual modes. Here the composite is made based on the sum of all strong northward-propagating events from May to October, divided by the number of years. Whereas the phase lag between the SST and convection is similar among all five modes, the amplitudes of the SST and convection in the positive IOB mode composite are largest. This is because for given the same intraseasonal SSTA forcing, the atmospheric wind and convection responses are stronger under a warmer basin-wide ocean surface condition. The strengthened convection and wind would lead to a greater SSTA. As a result, both the SST and convection perturbations could grow more rapidly during the positive IOB years than during other years.

It is worth mentioning that the IOB cases are selected based on a threshold of 0.7 standard deviation. We tested the sensitivity of the result to a different IOB threshold (say, 1.0 standard deviation). It turns out that both the IEPMIO and INPMIO analysis results are quite similar to those shown in Fig. 13 except with a higher confidence level under the IOB mode.

6 Summary

The effects of air–sea coupling over the TIO on the eastward and northward propagations of the BSISO and the modulation of air–sea coupling effect by Indian Ocean SST interannual variations were examined through diagnosing two 50-year simulations of the SINTEX-F CGCM. In the first simulation (CTL, the control experiment), the atmosphere and ocean are fully coupled. The second simulation (pdIO) excludes air–sea coupling in the TIO, instead forcing atmosphere with interannually varying monthly SST from the control simulation.

The SINTEX-F CGCM is capable of simulating realistic energy spectra, spatial–temporal evolutions and vertical structures of the eastward and northward propagations of the BSISO. It is noted that air–sea coupling over the TIO significantly enhances the eastward-propagating BSISO along the equator and the northward-propagating BSISO over the TIO. The maximum spectrum difference of the northward- (eastward-) propagating BSISO between the CTL and pdIO experiment reaches about 30% (25%) of the climatological values.

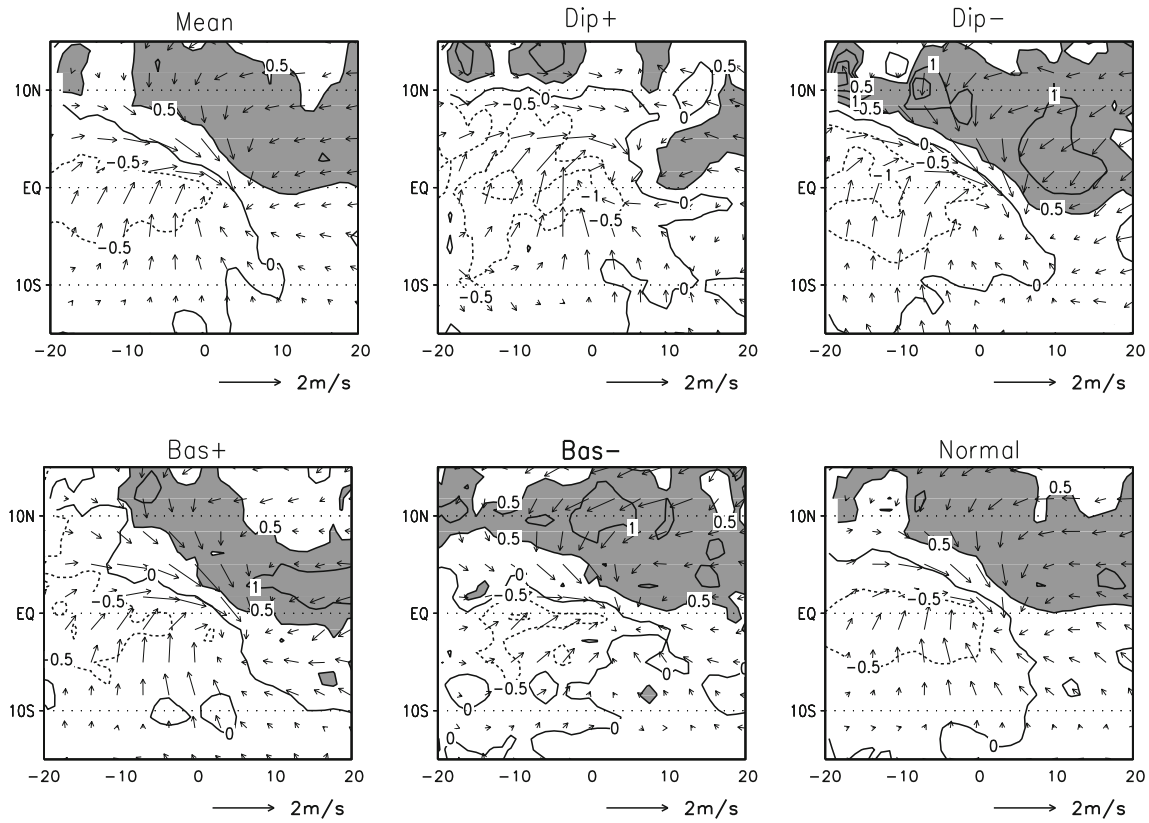

Fig. 16 Composite of the eastward propagating BSISO wind anomalies at 10-m (vector) and SSTA (*contour*, 10^{-1} K) for different interannual modes of Indian Ocean in the CTL. The composite is based on the following longitude locations, 60°, 70° and 80°E. Abscissa is the relative longitude (unit: longitudinal degree) with respect to the convection center. *Shading* represents SSTA greater than or equal to 0.5 (10^{-1} K)

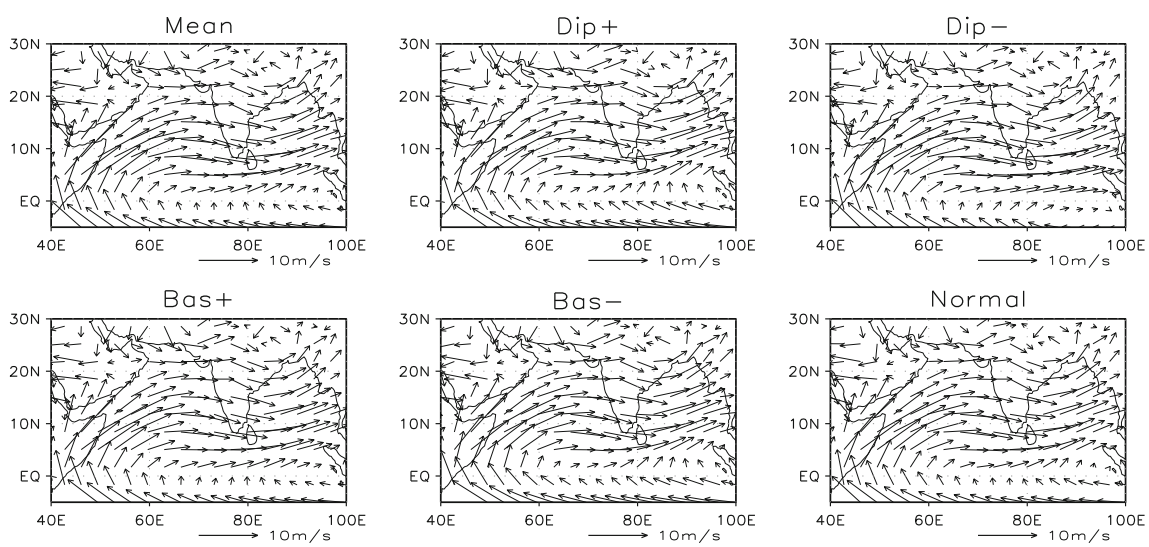

Fig. 17 Composite 850-hPa wind (m s^{-1}) fields during different Indian Ocean modes

Physical processes through which air–sea coupling affects the eastward and northward propagations of the BSISO are investigated. Air–sea coupling enhances the eastward-propagating intensity through a zonally asymmetric SST response. In boreal summer, the low-level background zonal wind along the equator is westerly. The

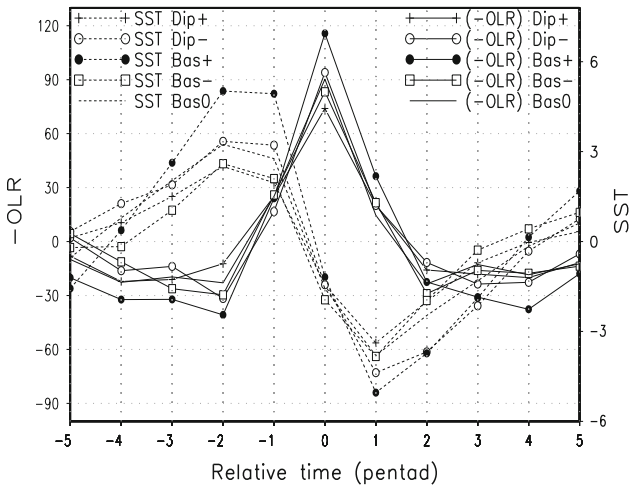

Fig. 18 Composite ISO convection (OLR, *solid line*, W m^{-2}) and SST (*dashed line*, 10^{-1} K) evolution with respect to the ISO convection center along 70°–95°E in the presence of various Indian Ocean modes. Abscissa is the relative time (pentad) with respect to the convection. The composite is based on multi latitudinal locations of the convection center within 5°–15°N

anomalous easterly to the east of the BSISO convection decreases the wind speed and thus surface evaporation, leading to a positive SSTA. The positive SSTA in turn forces a boundary-layer convergence, which further increases the boundary-layer humidity and atmospheric instability, enhancing the eastward propagation of the BSISO convection.

Similar air–sea feedback processes operate for the northward-propagating BSISO. The northward-propagating BSISO convection interacts with the monsoon westerly and the underlying ocean, generating a meridional asymmetric SST response (Fig. 11). The resultant positive SSTA north of the convection enhances the northward propagation intensity. The air–sea coupling also increases the background easterly shear, mean meridional moisture gradient and monsoon westerly, particularly over the Bay of Bengal (Fig. 12), which also favor the northward-propagating BSISO. As a large portion of the northward-propagating mode is connected to the eastward-propagating mode, the increased eastward-propagation BSISO (Fig. 3c) by air–sea coupling further enhances the northward-propagation BSISO.

A further analysis reveals that the aforementioned air–sea coupling effect can be modulated by the interannual SST variations over the TIO. The impact of air–sea coupling on eastward-propagating BSISO is enhanced during negative IOD, positive IOB and normal years, but weakened during positive IOD and negative IOB years. The cause of this phase dependence is attributed to the change of the background zonal wind in the equatorial Indian Ocean. The background westerly along the equator is enhanced during the negative IOD, positive IOB and normal years, but changes to a weak easterly during the positive IOD and negative IOB years. The SSTA averaged between 5°S and 5°N over the Indian Ocean is always positive to the east of the BSISO convection for all interannual modes, because the mean wind is always westerly north of the equator and because the ocean mixed layer depth is much shallower north of the equator than south of the equator over the TIO. Air–sea coupling reduces the zonal asymmetry of the low-level specific humidity and thus eastward propagation spectrum during the positive IOD and negative IOB modes. The cause of that is attributed to the wind-evaporation-SST feedback under the mean easterly at the equator. In pdIO with no local air–sea coupling, an anomalous easterly leads to an increase of the surface evaporation and the near surface humidity. In CTL with air–sea coupling involved, the enhanced surface evaporation leads to a local cooling that tends to reduce the surface evaporation through the modulation of the sea–air specific humidity difference. As a result, the coupling leads to a decrease of the humidity. An opposite air–sea coupling effect happens when the mean equatorial westerly is presented during the other interannual modes.

Different from the eastward propagation case, air–sea coupling always strengthens the northward-propagating BSISO in all five modes. This is because the key background variable that affects the air–sea coupling over the northern Indian Ocean is low-level westerly, which does not change sign under all interannual modes. The strongest enhancement happens during the positive IOB mode, possibly due to the enhanced air–sea coupling strength under warmer basin-wide background mean SST over the TIO.

It is worth emphasizing that the meridional asymmetry of low-level convergence and humidity fields in relevance to the BSISO convection exists even in the absence of air–sea interaction (Jiang et al. 2004). Air–sea coupling, on the other hand, strengthens the asymmetric amplitude through direct and indirect effects. The direct effect is through the change of intraseasonal SST. The indirect effect is through the change of seasonal mean state of atmospheric circulation. How air–sea coupling affects the atmospheric mean state is not clear at this moment and deserves further research.

In the pdIO run, interannual monthly SST forcing field was specified. It would be interesting to compare this case with a run forced by a daily SST field. Our previous result with a coarser resolution model (Fu et al. 2003) showed that an in-phase relation between the intraseasonal SST and rainfall fields exists in both daily and monthly SST forcing runs, which differs significantly from a lagged SST-rainfall phase relation in the coupled simulations and observations. It is expected that the overall spectrum differences between the CTL and pdIO may alter to a certain degree when a daily SST field is specified, even though the fundamental

features of the BSISO structure difference between the coupled and uncoupled simulations, particularly during different interannual TIO SST modes, may remain the same.

Most of previous studies showed that air–sea coupling generally increases the intensity of both the eastward and northward propagating ISO. However, its impact on the propagating speed is inconclusive: For example, Flatau et al. (1997) found that air–sea coupling slows down eastward-propagating ISO-like disturbances in their model. On the other hand, Watterson (2002) found that air–sea coupling speeds up the simulated eastward-propagating intraseasonal variability. It is also interesting to note that, in both the cases, air–sea coupling brings the model ISO propagation speed closer to the observed. Our previous modeling result (Fu et al. 2003) indicated that air–sea coupling significantly increases the strength of northward-propagating BSISO, but does not have a significant impact on the propagation speed. It is likely that the impact of air–sea coupling on the ISO propagation speed is model dependent. To comprehensively address this issue, multi-model inter-comparisons may be needed.

Acknowledgments This research was supported by NSFC Grant 41075073. TL was supported by ONR grants N000140810256 and N000141010774 and by the International Pacific Research Center that is sponsored by the Japan Agency for Marine-Earth Science and Technology (JAMSTEC), NASA (NNX07AG53G) and NOAA (NA17RJ1230). This is SOEST contribution number 8048 and IPRC contribution number 736.

References

Ajayamohan RS, Rao SA, Yamagata T (2008) Influence of Indian Ocean dipole on poleward propagation of boreal summer intraseasonal oscillations. J Clim 21:5437–5454

Ajayamohan RS, Rao SA, Luo J-J, Yamagata T (2009) Influence of Indian Ocean dipole on boreal summer intraseasonal oscillations in a coupled general circulation model. J Geophys Res 114: D06119. doi:10.1029/2008JD011096

Ashok K, Guan Z, Yamagata T (2001) Impact of the Indian Ocean dipole on the relationship between the Indian monsoon rainfall and ENSO. Geophys Res Lett 28:4499–4502

Bellon G, Sobel AH (2008) Instability of the axisymmetric monsoon flow and intraseasonal oscillation. J Geophys Res 113:D07108. doi:10.1029/2007JD009291

Bellon G, Sobel AH, Vialard J (2008) Ocean–atmosphere coupling in the monsoon intraseasonal oscillation: a simple model study. J Clim 21:5254–5270

Chang C-P, Li T (2000) A theory of the tropical tropospheric biennial oscillation. J Atmos Sci 57:2209–2224

Chen T-C, Murakami M (1988) The 30–50 day variation of convective activity over the western Pacific Ocean with the emphasis on the northwestern region. Mon Wea Rev 116:892–906

Chen X, Wang H, Zeng Q (2000) Atmospheric intraseasonal oscillation and its interannual variation. Beijing China Meteorological Press, Beijing, p 176

Cherchi A, Gualdi S, Behera S, Luo JJ, Masson S, Yamagata T, Navarra A (2007) The influence of tropical Indian Ocean SST on the Indian Summer Monsoon. J Clim 20:3083–3105

Drbohlav H-K, Wang B (2005) Mechanism of the northward-propagating intraseasonal oscillation: insights from a zonally symmetric model. J Clim 18:952–972

Flatau M, Flatau PJ, Phoebus P, Niller PP (1997) The feedback between equatorial convection and local radiative and evaporative processes: the implications for intraseasonal oscillations. J Atmos Sci 54:2373–2386

Fu X, Wang B (2004) The boreal-summer intraseasonal oscillations simulated in a hybrid coupled atmosphere–ocean model. Mon Wea Rev 132:2628–2649

Fu X, Wang B, Li T, McCreary JP (2003) Coupling between northward- propagating, intraseasonal oscillations and sea surface temperature in the Indian Ocean. J Atmos Sci 60:1733–1753

Fu X, Wang B, Waliser DE, Tao L (2007) Impact of atmosphere–ocean coupling on the predictability of monsoon intraseasonal oscillations. J Atmos Sci 64:157–174

Fu X, Wang B, Bao Q, Wang B (2008) Sea surface temperature feedback extends the predictability of tropical intraseasonal oscillation. Mon Wea Rev 136:577–597

Gualdi S, Navarra A, Guilyardi E, Delecluse P (2003) Assessment of the tropical Indo-Pacific climate in the SINTEX CGCM. Ann Geophys 46:1–26

Guilyardi E, Delecluse P, Gualdi S, Navarra A (2003) Mechanisms for ENSO phase change in a coupled GCM. J Clim 16:1141–1158

Hayashi Y (1982) Space–time spectral analysis and its applications to atmospheric waves. J Meteorol Soc Japan 60:56–171

Hendon HH (2000) Impact of air–sea coupling on the Madden–Julian oscillation in a general circulation model. J Atmos Sci 57:3939–3952

Hong C-C, Li T, Kug J-S, Lin Ho (2008a) Asymmetry of the Indian Ocean dipole. Part I: observational analysis. J Clim 21:4834–4848

Hong C-C, Li T, Luo J-J (2008b) Asymmetry of the Indian Ocean dipole. Part II: model diagnosis. J Clim 21:4849–4858

Hong C-C, Li T, Lin H, Chen Y-C (2010) Asymmetry of the Indian Ocean Basin-wide SST Anomalies: roles of ENSO and IOD. J Clim (in press)

Hsu PC, Li T (2010) Interactions between boreal summer intraseasonal oscillations and synoptic-scale disturbances over the western North Pacific. Part II: apparent heat and moisture sources and eddy momentum transport. J Clim (in press)

Hsu PC, Li T, Tsou C-H (2010) Interactions between boreal summer intraseasonal oscillations and synoptic-scale disturbances over the western North Pacific. Part I: energetics diagnosis. J Clim (in press)

Inness PM, Slingo JM (2003) Simulation of the Madden–Julian oscillation in a coupled general circulation model. Part I: comparison with observations and an atmosphere-only GCM. J Clim 16:345–364

Jiang X, Li T, Wang B (2004) Structures and mechanisms of the northward propagating boreal summer intraseasonal oscillations. J Clim 17:1022–1039

Joseph PV, Sabin TP (2008) An ocean–atmosphere interaction mechanism for the active break cycle of the Indian summer monsoon. Clim Dyn 30(6):553–566. doi:10.1007/s00382-007-0305-2

Ju J, Qian C, Cao J (2005) The intraseasonal oscillation of East Asian summer monsoon. Chinese J Atmos Sci (in Chinese) 29:187–194

Kemball-Cook S, Wang B (2001) Equatorial waves and air–sea interaction in the boreal summer intraseasonal oscillation. J Clim 14:2923–2942

Kemball-Cook S, Wang B, Fu X (2002) Simulation of the intraseasonal oscillation in ECHAM-4 model: the impact of coupling with an ocean model. J Atmos Sci 59:1433–1453

Krishnamurti TN, Subrahmanyam D (1982) The 30–50 day mode at 850 mb during MONEX. J Atmos Sci 39:2088–2095

Lau K-M, Chan PH (1986) Aspects of the 40–50 day oscillation during the northern summer as inferred from outgoing longwave radiation. Mon Wea Rev 114:1354–1367

Lau K–M, Yang S (1996) Seasonal variation, abrupt transition and intraseasonal variability associated with the Asian summer monsoon in the GLA GCM. J Clim 9:965–985

Li T, Wang B (1994) The influence of sea surface temperature on the tropical intraseasonal oscillation: a numerical study. Mon Wea Rev 122:2349–2362

Li T, Zhang Y (2002) Processes that determine the quasi-biennial and lower-frequency variability of the South Asian monsoon. J Meteorol Soc Japan 80:1149–1163

Li T, Zhou C (2009) Planetary scale selection of the Madden–Julian Oscillation. J Atmos Sci 66:2429–2443

Li T, Zhang YS, Chang C-P, Wang B (2001) On the relationship between Indian Ocean SST and Asian summer monsoon. Geophys Res Lett 28:2843–2846

Li C, Long Z, Mu M (2003a) Atmospheric intraseasonal oscillation and its important effect. Chinese J Atmos Sci (in Chinese) 27:518–535

Li T, Wang B, Chang C-P, Zhang Y (2003b) A theory for the Indian Ocean dipole-zonal mode. J Atmos Sci 60:2119–2135

Li T, Tam F, Fu X, Zhou T, Zhu W (2008) Causes of the intraseasonal SST variability in the tropical Indian Ocean. Atmos Ocean Sci Lett 1:18–23

Liebmann B, Smith CA (1996) Description of a complete (interpolated) outgoing longwave radiation dataset. Bull Am Meteorol Soc 77:1275–1277

Lin A, Li T (2008) Energy spectrum characteristics of boreal summer intraseasonal oscillations: climatology and variations during the ENSO developing and decaying phases. J Clim 21:6304–6320

Lin A, Wan Q, Liang J, Yuan J (2004) Influence of tropical southwest monsoon on tropical cyclone Vongfong (0214). Acta Meteorol Sinica (in Chinese) 62:841–850

Lin A, Liang J, Li C, Gu D, Zheng B (2007) Monsoon circulation background of '0506' continuous rainstorm in South China. Adv Water Sci (in Chinese) 18:424–432

Lin A, Li T, Li C (2010) Relationships between interannual anomalies of sea surface temperature in the Indian Ocean and tropical boreal summer intraseasonal oscillations: observations and simulations. Acta Meteorol Sinica (in Chinese) 68:617–630

Lindzen RS, Nigam S (1987) On the role of sea surface temperature gradients in forcing low-level winds and convergence in the tropics. J Atmos Sci 44:2418–2436

Luo J-J, Masson S, Behera S, Delecluse P, Gualdi S, Navarra A, Yamagata T (2003) South Pacific origin of the decadal ENSO-like variation as simulated by a coupled GCM. Geophys Res Lett 30:2250. doi:10.1029/2003GL018649

Luo J-J, Masson S, Roeckner E, Madec G, Yamagata T (2005a) Reducing climatology bias in an ocean–atmosphere CGCM with improved coupling physics. J Clim 18:2344–2360

Luo J-J, Masson S, Behera S, Shingu S, Yamagata T (2005b) Seasonal climate predictability in a coupled OAGCM using a different approach for ensemble forecasts. J Clim 18:4474–4497

Luo J-J, Masson S, Behera S, Yamagata T (2007) Experimental forecasts of the Indian Ocean dipole using a coupled OAGCM. J Clim 20:2178–2190

Luo J-J, Masson S, Behera S, Yamagata T (2008a) Extended ENSO predictions using a fully coupled ocean–atmosphere model. J Clim 21:84–93

Luo J-J, Behera S, Masumoto Y, Sakuma H, Yamagata T (2008b) Successful prediction of the consecutive IOD in 2006 and 2007. Geophys Res Lett 35:L14S02. doi:10.1029/2007GL032793

Luo J-J, Zhang R, Behera SK, Masumoto Y, Jin F-F, Lukas R, Yamagata T (2010) Interaction between El Niño and extreme Indian Ocean dipole. J Clim 23:726–742

Madden RA, Julian PR (1971) Detection of a 40–50 day oscillation in the zonal wind in the tropical Pacific. J Atmos Sci 28:702–708

Madden RA, Julian PR (1972) Description of global-scale circulation cells in the tropics with a 40–50 day period. J Atmos Sci 29:1109–1123

Madden RA, Julian PR (1994) Observation of the 40 50 day tropical oscillation- a review. Mon. Wea. Rev. 122:814–837

Madec G, Delecluse P, Imbard M, Levy C (1998) OPA 8.1 ocean general circulation model reference manual. LODYC/IPSL technical report note 11, Paris, France, p 91

Newman M, Sardeshmukh PD, Penland C (2009) How important is air–sea coupling in ENSO and MJO evolution? J Clim 22:2958–2977

Saji NH, Goswami BN, Vinayachandran PN et al (1999) A dipole in the tropical Indian Ocean. Nature 401:360–363

Sengupta D, Ravichandran M (2001) Oscillations of Bay of Bengal sea surface temperature during the 1998 summer monsoon. Geophys Res Lett 28:2033–2036

Sengupta D, Goswami BN, Senan R (2001) Coherent intraseasonal oscillations of ocean and atmosphere during Asian summer monsoon. Geophys Res Lett 28:4127–4130

Seo K-H, Schemm J-K, Jones C, Moorthi S (2005) Forecast skill of the Tropical Intraseasonal Oscillation in the NCEP GFS dynamical extended range forecasts. Clim Dyn 25:265–284

Seo Kyong-Hwan, Schemm Jae-Kyung E, Wang Wanqiu, Kumar Arun (2007) The boreal summer intraseasonal oscillation simulated in the NCEP climate forecast system: the effect of sea surface temperature. Mon Wea Rev 135:1807–1827

Seo Kyong-Hwan, Wang Wanqiu, Gottschalck Jon, Zhang Qin, Schemm Jae-Kyung E, Higgins Wayne R, Kumar Arun (2009) Evaluation of MJO forecast skill from several statistical and dynamical forecast models. J Clim 22:2372–2388

Shi X, Ding Y (2000) A study on extensive heavy rain processes in south China, the summer monsoon activity in (1994). Acta Meteorol Sinica (in Chinese) 58:666–678

Shinoda T, Han W (2005) Influence of the Indian Ocean dipole on atmospheric subseasonal variability. J Clim 18:3891–3909

Tan Y, Zhang R, He J (2003) Features of the interannual variation of sea surface temperature anomalies and the air–sea interaction in tropical Indian Ocean. Chinese J Atmos Sci (in Chinese) 27(1):53–66

Teng H, Wang B (2003) Interannual variations of the boreal summer intraseasonal oscillation in the Asian-Pacific region. J Clim 16:3571–3584

Torrence Cristopher, Compo Gilbert P (1998) A practical guide to wavelet analysis. Bull Am Meteorol Soc 79(1):61–78

Valcke S, Terray L, Piacentini A (2000) The OASIS coupler user guide version 2.4. CERFACE technical report TR/CGMC/00-10, p 85

Vecchi G, Harrison DE (2002) Monsoon breaks and subseasonal sea surface temperature variability in the Bay of Bengal. J Clim 15:1485–1493

Waliser DE, Lau KM, Kim JH (1999) The influence of coupled sea surface temperatures on the Madden–Julian oscillation: a model perturbation experiment. J Atmos Sci 56:333–358

Wang B (2006) The Asian Monsoon, intraseasonal variability. In: Waliser DE (eds) Springer Praxis, Chichester, pp 203–257

Wang B, Rui H (1990) Synoptic climatology of transient tropical intraseasonal convection anomalies: 1975–1985. Meteorol Atmos Phys 44:43–61

Wang B, Xie X (1997) A model for the boreal summer intraseasonal oscillation. J Atmos Sci 54:72–86

Wang B, Xie X (1998) Coupled modes of the warm pool climate system. Part I: the role of air–sea interaction in maintaining Madden–Julian Oscillation. J Clim 11:2116–2135

Wang B, Webster Peter, Kikuchi Kazuyoshi et al (2006) Boreal summer quasi-monthly oscillation in the global tropics. Clim Dyn 27:661–675

Watterson IG (2002) The sensitivity of subannual and intraseasonal tropical variability to model ocean mixed layer depth. J Geophys Res 107(D2):4020. doi:10.1029/2001JD000671

Webster PJ (1983) Mechanisms of monsoon low-frequency variability: surface hydrological effects. J Atmos Sci 40:2110–2124

Wu ML, Schubert S, Kang IS, Waliser DE (2002) Forced and free intraseasonal variability over the south Asian monsoon region simulated by 10 AGCMs. J Clim 15:2862–2880

Wu B, Zhou T, Li T (2009) Seasonally evolving dominant interannual variability modes of East Asian climate. J Clim 22:2992–3005

Wu B, Li T, Zhou T (2010) Relative contributions of the Indian Ocean and local SST anomalies to the maintenance of the western North Pacific anomalous anticyclone during El Niño decaying summer. J Clim 23:2974–2986

Xie SP, Hu K, Hafner J, Tokinaga H, Du Y, Huang G, Sampe T (2009) Indian Ocean capacitor effect on Indo–Western Pacific climate during the summer following El Niño. J Clim 22:730–747

Yamagata T, Behera S, Luo J-J, Masson S, Jury M, and Rao SA (2004) Coupled ocean–atmosphere variability in the tropical Indian Ocean. Earth's climate: the ocean–atmosphere interaction. Geophysics monograph, vol 147. American geophysics union, pp 189–212

Yang M, Ding Y (2007) A study of the impact of South Indian Ocean dipole on the summer rainfall in China. Chinese J Atmos Sci (in Chinese) 31(4):685–694

Yasunari T (1979) Cloudiness fluctuations associated with the Northern Hemisphere summer monsoon. Meteorol Soc Japan 57:227–242

Zheng Y, Waliser DE, Stern WF, Jones C (2004) The role of coupled sea surface temperatures in the simulation of the tropical intraseasonal oscillation. J Clim 17:4109–4134

Zhou C, Li T (2010) Upscale feedback of tropical synoptic variability to intraseasonal oscillations through the nonlinear rectification of the surface latent heat flux. J Clim (in press)

Zhu C, Nakazawa T, Li J (2004) Modulation of tropical depression/cyclone over the Indian–western pacific oceans by madden–julian oscillation. Acta Meteorol Sinica (in Chinese) 62:42–50